

Coherence of a charge stabilised tin-vacancy spin in diamond

Johannes Görlitz¹, Dennis Herrmann¹, Philipp Fuchs¹, Takayuki Iwasaki²,
Takashi Taniguchi³, Detlef Rogalla⁴, David Hardeman⁵, Pierre-Olivier Colard⁵,
Matthew Markham⁵, Mutsuko Hatano², Christoph Becher^{1*}

October 12, 2021

¹Fachrichtung Physik, Universität des Saarlandes, Campus E2.6, D-66123 Saarbrücken, Germany

²Department of Electrical and Electronic Engineering, Tokyo Institute of Technology, Meguro, Tokyo 152-8552, Japan

³International Center for Materials Nanoarchitectonics, National Institute for Materials Science, 1-1 Namiki, Tsukuba 305-0044, Japan

⁴RUBION, Ruhr-Universität Bochum, Universitätsstraße 150, D-44801 Bochum, Germany

⁵Element Six Global Innovation Centre, Fermi Avenue, Harwell Oxford, Didcot, Oxfordshire, OX11 0QR, United Kingdom

Abstract

Quantum information processing (QIP) with solid state spin qubits strongly depends on the efficient initialisation of the qubit's desired charge state. While the negatively charged tin-vacancy (SnV^-) centre in diamond has emerged as an excellent platform for realising QIP protocols due to long spin coherence times at liquid helium temperature and lifetime limited optical transitions, its usefulness is severely limited by termination of the fluorescence under resonant excitation [1, 2, 3]. Here, we unveil the underlying charge cycle of group IV-vacancy (G4V) centres and exploit it to demonstrate highly efficient initialisation of the desired negative charge state of single SnV centres while preserving long term stable optical resonances. We furthermore all-optically probe the coherence of the ground state spins by means of coherent population trapping and find a spin dephasing time of $5(1)\mu\text{s}$. Additionally, we demonstrate proof-of-principle single shot spin state readout without the necessity of a magnetic field aligned to the symmetry axis of the defect.

Introduction

Colour centres in diamond have recently emerged as competitive platforms in the field of QIP [4, 5, 6]. In particular the G4V centres combine long spin coherence times [1, 7] with favourable optical properties such as large Debye-Waller factors [2, 8] and transform limited resonance linewidths [2, 3, 9, 10]. While the large spectral diffusion for the nitrogen vacancy centre in diamond [11] is to be expected, G4V centres should be protected by their inversion symmetry from large first order Stark shifts. Nevertheless, spectral diffusion due to second order effects is still common to impose a strong limit on the usefulness in quantum information and simulation applications [3, 12, 13, 14, 15, 16], which makes overcoming these spectral instabilities a crucial task. The origin of the unstable resonance lines is oftentimes introduced by fluctuating charges resulting from impurities or lattice defects in the vicinity of the colour centre. Furthermore, these environmental impurities and defects can act as charge traps or electron donors leading to an ill-defined charge state of the emitter. Among the G4V centres, the SnV^- centre [2, 17, 18, 19] shows great promise in terms of spin coherence at easily accessible liquid helium temperatures [1] and lifetime limited optical transitions [2, 3]. Unfortunately, its potential for application in QIP is suffering strongly from the termination of fluorescence under resonant excitation [1, 2, 3]. In this work, we investigate the mechanism leading to the charge instability of a single SnV^- centre in diamond and find it to be a single photon process. We furthermore fully explore the charge cycle of the SnV centre and use it to implement a straightforward, highly efficient initialisation of the negative charge state while preserving longterm stability of dipole allowed optical transitions. We find that the principle of this charge cycle can also directly be applied to other G4V centres for efficient

control of their charge state. Subsequently, we probe the coherence of the charge stabilised SnV^- centre by an all-optical coherent population trapping (CPT) scheme, yielding a spin dephasing time of the ground state of $T_2^* = 5(1) \mu\text{s}$. By employing a proof-of-principle single shot readout protocol, we demonstrate the presence of highly cycling optical transitions even in the case of large angles between the magnetic field and the symmetry axis of the defect.

Results

Charge cycle of the SnV^- centre

We investigate single SnV^- centres in diamond created upon ion implantation (see method section for details on the sample and the experimental setup) at temperatures of 2 K, for which termination of fluorescence is reliably observed under resonant excitation of the defect [1, 2, 3]. Without additional measures, we find this termination to be permanent, even after hour long waiting times in the dark. Furthermore, by performing resonant excitation scans over a large spectral range of several GHz, we can exclude that the resonance line is simply shifted due to spectral diffusion, the range of which is typically limited to $\ll 1$ GHz for the SnV^- centre. Applying an additional 532 nm laser pulse, as often used in experiments with G4V centres, suffices to recover the fluorescence, but usually leads to a resonance line shifted by up to several hundred MHz [2], much larger than the typical lifetime-limited linewidths of 20-30 MHz. A similar effect was also found for germanium vacancy centres in diamond [20]. These spectral shifts impose a strong limitation on the usefulness of the SnV^- centre in QIP. The origin of the instability of the resonance line is most likely caused by an altered charge environment after the application of the 532 nm laser. Understanding these charge dynamics is crucial in order to fully exploit the superior spin coherence of single SnV^- centres at liquid helium temperatures compared to other G4V centres [1, 7, 17, 21, 22].

In order to stabilise the desired negative charge state of the SnV centre without inducing spectral shifts, we systematically vary the wavelength of an additionally applied light field. To this end we perform a measurement in which we use a continuous wave dye laser to resonantly excite an ensemble of SnV^- centres on the C-transition (see Fig.1c), add a second light field provided by a pulsed supercontinuum laser source at a repetition rate of 80 MHz and monitor the count rate on the phonon sideband (Bandpass filter: 655(47) nm). We scan the wavelength of the second laser from 420 nm up to 580 nm with a spectral bandwidth of 10 nm while keeping the power fixed and compare the count rate of the purely resonant excitation to the count rate of the two-colour excitation while subtracting the counts caused by the second light field alone (Fig.1b)). For wavelengths of the second light field $\gtrsim 520$ nm the ensemble fluorescence remains at a low level due to the fluorescence termination discussed above. However, we observe a fluorescence enhancement starting at wavelengths (energies) shorter (larger) than 520 nm (2.4 eV) for which we define the enhancement factor as the ratio between counts with and without the second laser. The observed fluorescence enhancement indicates a stabilisation of the desired negative charge state for photon energies above 2.4 eV, hinting at a charge transfer process occurring at a certain threshold. This result is confirmed by a similar measurement on a second HPHT sample, see supplemental material. Before devising a model for the SnV charge cycle, we further investigate the charge dynamics. To this end, we select 445 nm as the optimised wavelength for recovery of the negative charge state of the SnV centre, because it lies at the optimum of fluorescence enhancement while minimising the direct excitation of the SnV^- centre. We now evaluate the number of photons that are taking part in the charge transfer process under resonant excitation. To this end, we employ a 10 ms laser pulse at 445 nm to initialise the negative charge state of a single SnV^- centre (Emitter 1, characterisation of the single photon emission can be found in the supplemental material). Subsequently, we apply a 1 s long laser pulse resonant with the C-transition of the defect and collect photons emitted into the phonon sideband. The duration of the resonant laser pulse is chosen sufficiently long such that charge transfer will occur during this time even for the lowest power used. An exemplary excerpt of such a time trace is depicted in Fig.2a). We repeat this measurement about 500 times for each laser power and extract the charge state lifetime, which we define as the duration until charge transfer occurs under resonant excitation, by evaluating the duration of emission of the SnV^- centre until the fluorescence is terminated. A histogram of such a measurement and the extracted lifetime is shown in Fig.2b). The inverse of the lifetime yields the charge transfer rate, which increases linearly with the resonant excitation power (see Fig.2c)). We therefore conclude that charge transfer occurs as

a single photon process. It takes place when the SnV^- centre is in the excited state, since termination of fluorescence does not occur when the excitation laser is far detuned from resonance. In such a case one would intuitively expect a two photon process where the first photon excites the emitter and the second photon causes the charge transfer, therefore leading to a quadratic power dependence of the charge transfer rate. However, the charge transfer happens at time scales much longer (6 orders of magnitude) than the lifetime of the excited state. We thus expect that the charge transfer starts from a steady state population of the excited state created by the resonant excitation and consequently involves only a single photon.

To explain the charge transfer processes occurring under resonant excitation and illumination with a second light field we start with the position of the energy levels of the SnV^- centre in the diamond bandgap (Fig.1a)). All numbers are taken from theoretical calculations of [19]. The highest occupied levels of the SnV^- excited state lie $0.6\text{eV}+2.0\text{eV}$ above the valence band and thus $5.47\text{eV}-2.6\text{eV}=2.87\text{eV}$ below the conduction band.

We exclude a charge transfer process under resonant illumination by photo-ionization of an electron from the excited state to the conduction band based on the following facts and observations: (i) the photon energy of 2.0eV is not sufficient for a one photon-excitation from the excited state to the conduction band; (ii) a two-photon process from the excited state ($2\cdot 2.0\text{eV}>2.87\text{eV}$) is excluded as we observe a one-photon charge transfer process (see discussion above); (iii) electron ionisation would leave the SnV center in its neutral state. Although it is very challenging to unambiguously observe emission from different charge states (due to potential charge transfer happening upon excitation) we gather evidence against transfer into the neutral charge state: When exciting an ensemble of SnV^- centres resonantly without any charge stabilising laser being applied and measuring spectra integrated longer than 10 min in the spectral region from 620-900 nm, these measurements do not show the slightest hint of SnV^0 centre emission, which is theoretically predicted to lie at 680(40) nm [23]. Transfer of a single charge then only leaves the alternative of transfer to the doubly negative charge state SnV^{2-} which is an optically inactive state and cannot be observed spectroscopically. However, our combined observations as discussed above lead to the conclusion that the dark state of the SnV centre is indeed the SnV^{2-} . This claim furthermore is in agreement with recent experimental findings on the SiV^- center where a doubly negative charge state was identified as the dark state [24].

We here go a step further and propose a model which not only explains the SnV centre charge dynamics but should be generally valid for all G4V centers. Our model is based on the charge state conversion process identified in [24], i.e. capture of an electron from the valence band (hole generation) for the $\text{SnV}^- \rightarrow \text{SnV}^{2-}$ process and release of an electron to a hole in the valence band (hole capture) for going from $\text{SnV}^{2-} \rightarrow \text{SnV}^-$. The latter process requires the presence of a valence band hole in the vicinity of the SnV center which might be created by another close-by defect upon photo-excitation. We identify this defect by the measurement of fluorescence enhancement presented in Fig.1b): The onset and also the shape of the fluorescence enhancement curve agree very well with the theoretically proposed [25] and experimentally confirmed [26] charge transition of the neutral divacancy in diamond to its negative charge state. This charge transition occurs due to promotion of an electron from the valence band to the divacancy [25, 26]. It was also reported, that the efficiency of this ionisation reaches unity charge conversion at photon energies $>3\text{eV}$. The diamond sample investigated in this study is very likely to contain many divacancies even after the HPHT annealing [27], since the implantation of heavy tin ions creates a massive amount of vacancies which tend to form divacancies in an exothermic reaction during annealing due to single vacancies becoming mobile [28]. Based on these considerations we propose the following charge cycle for the SnV^- centre: A resonant 620 nm (2eV) photon first excites the SnV^- centre to a fully occupied e_g state (see Fig.1a)). A subsequent 620 nm photon promotes an electron from the valence band to the SnV^- centre's empty e_u orbital and transforms it into its optically inactive charge state SnV^{2-} . A photon with a wavelength (energy) of 420-520 nm ($2.4\text{-}3\text{eV}$) excites an electron from the valence band to a defect in the diamond lattice, the most likely candidate being the neutral divacancy. This process creates a hole in the valence band which diffuses towards the SnV^{2-} centre where a recombination leads to the return to SnV^- , which closes the cycle. This scheme is also suitable to explain the large spectral shifts that occur when applying 532 nm laser light as a charge repump. The energy of the light is not sufficient to efficiently convert all the surrounding divacancies to their negative charge state and therefore leaves an ill-defined charge environment.

Building on these results, we evaluate the efficiency with which we can initialise the negative charge state of the investigated SnV centre. For this we apply a 445 nm initialisation pulse with variable pulse

length and a cw power of $50 \mu\text{W}$ which is followed by a 0.5 s resonant laser pulse creating a fluorescence response if the SnV^- charge state is properly initialised. The power of the resonant laser pulse is chosen corresponding to an electron capture rate of 46 Hz (blue dot in Fig.2c) ensuring electron capture with more than 99.9% probability. For each blue pulse length, we repeat the measurement about 250 times and count the number of initialisation pulses after which a fluorescence response is observable. The ratio of observed pulses to the total number of pulses used yields the initialisation efficiency, which is depicted in Fig.2d). We reach a saturation value of 91(1)% charge initialisation, which follows an exponential growth law resulting from pumping the electron from the valence band to the neutral divacancy and subsequent hole capture of the SnV^{2-} . 4(1)% of the missing efficiency are due to the number of pulses where electron capture occurs too fast to create a sufficiently strong fluorescence response to be distinguished from the dark counts and background in our system. The last 5% to unity might be caused by spurious electron capture by the blue laser itself. It is worth noting, that we found this concept of initialisation to work on every emitter that we investigated in this sample and a similar HPHT annealed second sample (see supplementary material). Detailed results of a second emitter under investigation reaching 97% of charge state initialisation efficiency can be found in the supplementary information. Further results on the photophysics of SnV^- centres in low-pressure-low-temperature annealed diamond samples which are induced by the charge cycle described above will be published elsewhere.

We would furthermore like to emphasise that the proposed charge cycle model and the method for stabilising the negative charge state are most probably universal to the G4V centers in diamond. The reason is that their general electronic level structure is identical and the lower e_u orbitals generally lie close to the valence band edge such that the charge transfer as discussed here for SnV centres works in an analogous fashion. Small differences might evolve due to different concentrations of divacancies introduced in the implantation process and absolute energy positions within the band gap of diamond. This claim is strongly supported by an experiment on a resonantly excited ensemble of SiV^- centres in which a very similar fluorescence enhancement under illumination with a second tunable laser is observed (see supplemental material) and furthermore by the findings reported in [24].

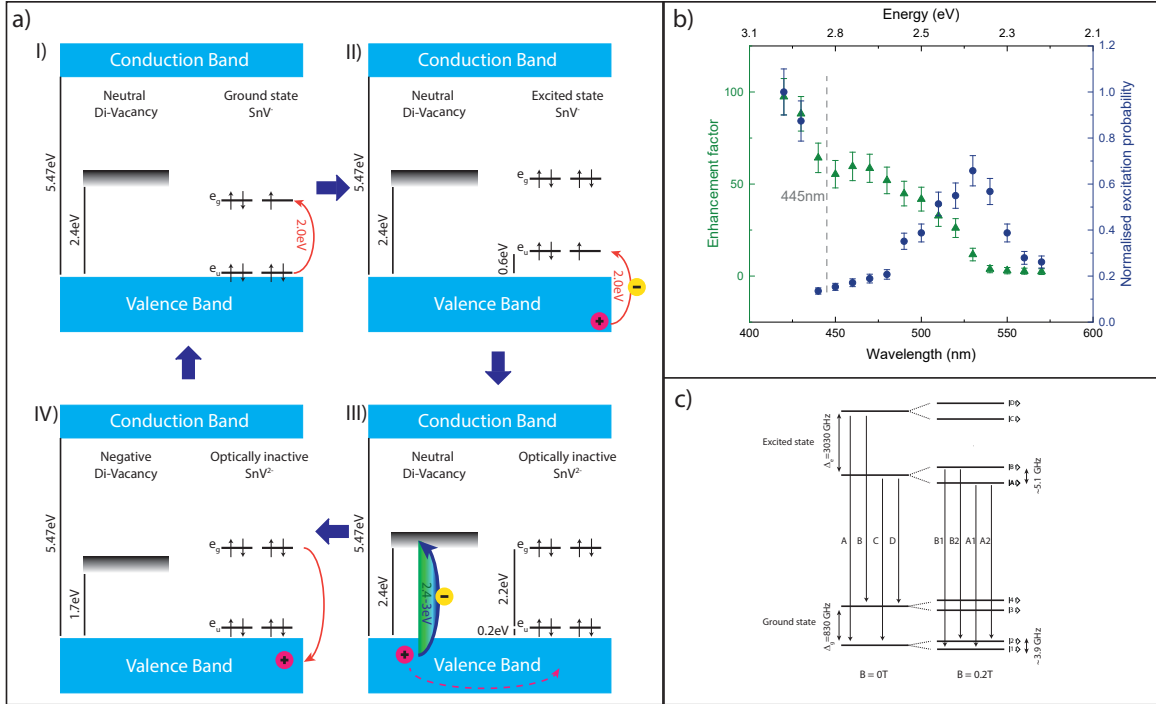


Figure 1: **Charge processes of the SnV⁻ centre:** **a)** Proposed scheme for the charge cycle of the SnV⁻ centre. In I) the SnV⁻ centre gets excited by a resonant 2 eV photon. In II) a second 2 eV photon promotes an electron from the valence band to the SnV⁻ centre, transforming it into its optically inactive charge state SnV²⁻. In III) a photon with an energy above 2.4 eV drives the charge transition of a defect in the diamond lattice, most likely the neutral divacancy. In this process a hole is created in the valence band which diffuses in IV) towards the SnV²⁻ centre, where a recombination takes place. All absolute energy positions related to the charge states of the SnV⁻ centre are extracted from [19]. **b)** Enhancement of fluorescence factor of an ensemble of SnV⁻ centres, excited resonantly on the C-transition and under addition of a second laser with tunable wavelength. The enhancement factor is defined as the ratio between counts with and without the second laser. For comparison, the normalised excitation probability measured via excitation by the second laser only is plotted. The excitation probability peaks at 2.4 eV due to excitation to a higher excited state of the SnV⁻ [2] and an indication of an even higher lying excited state is seen at photon energies larger 2.8 eV most likely resulting from a deeper lying electron state in the valence band [19]. **c)** Fine structure and Zeeman splitting of the SnV⁻ centre. The relevant optical transitions and splittings at B=0 T and B=0.2 T for this work are labeled.

Long term stability of the resonances of a charge stabilised SnV(-)

The ability to reliably initialise the negative charge state of the SnV⁻ centre enables us to investigate the influence of spectral diffusion on the long term stability of the electronic transitions. The spectral diffusion can have two different origins: Firstly, fluctuations in the charge environment that introduce Stark shifts [13] even while no charge transfer is induced (e.g. the negative charge state is preserved) and secondly, shifts in the spectral position that only occur while electron capture and the subsequent charge cycle of the defect are happening. The difference between the two cases is, while for a preserved negative charge state only fluctuations in the potentially far distance charge environment influence the spectral stability, for the SnV undergoing one full charge cycle it is not guaranteed that the near scale charge environment will end up in its original state. Therefore, we expect stronger influence on the spectral diffusion in the latter case. In order to separate the two effects, we perform photoluminescence excitation (PLE) spectroscopy and use very low excitation powers below 0.5 nW in order to avoid power broadening and electron capture. In this way, one can resolve very small spectral shifts on the order of the natural linewidth of about 25 MHz that are only caused by environmental fluctuations. During the

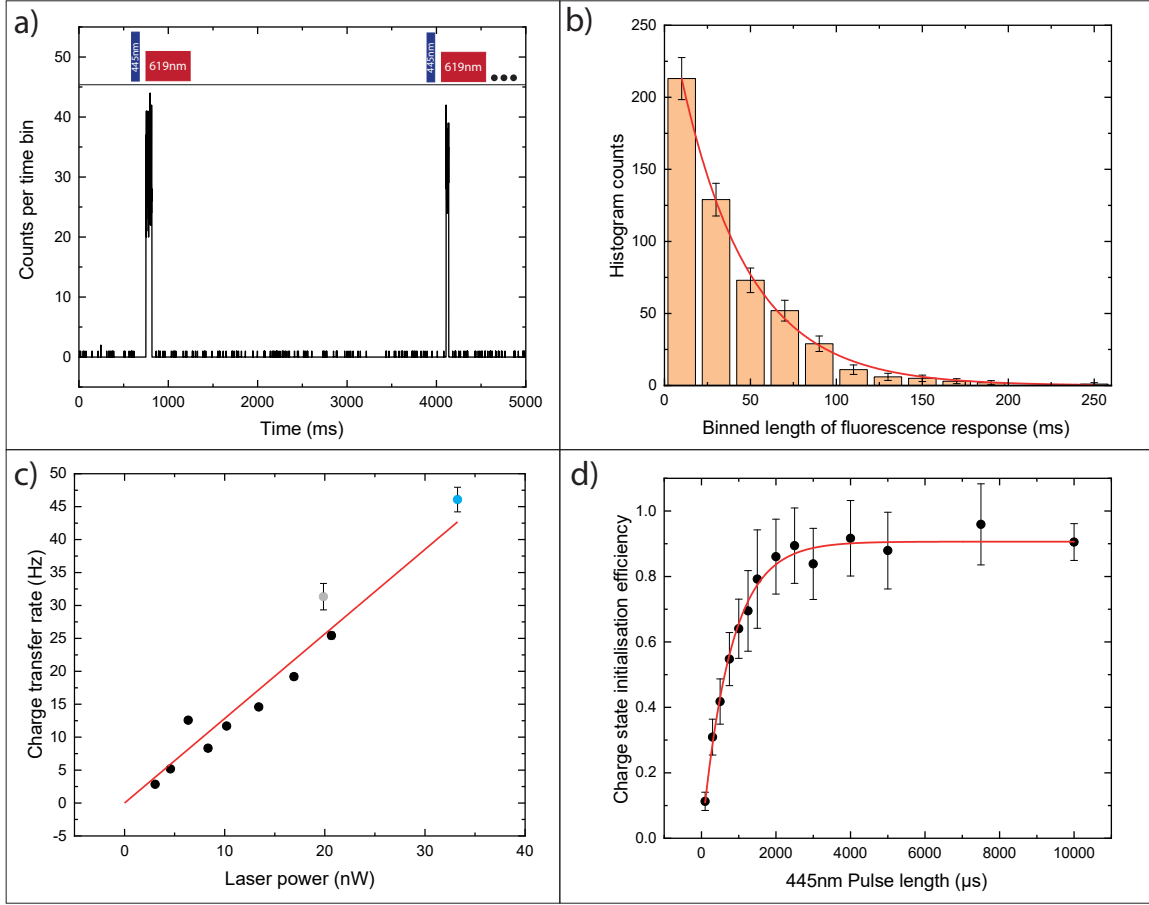


Figure 2: **Electron capture and charge initialisation of a single SnV^- centre:** **a)** Exemplary part of a measurement sequence of the charge initialisation and electron capture experiments on a single SnV^- centre (Emitter 1). After the 10 ms laser pulse at 445 nm initialises the charge state, a fluorescence response by the 1 s long resonant laser pulse on the C-transition is visible. The fluorescence response lasts until electron capture occurs. **b)** Histogram of the lengths of the fluorescence responses for a given resonant laser power of 20.7 nW. An exponential fit yields the charge state lifetime until charge transfer occurs. This lifetime translates directly to an charge transfer rate for every given laser power. **c)** Charge transfer rate plotted against the resonant excitation laser power. The linear dependence of the charge capture rate on the power indicates a single photon process from the excited state, since termination of fluorescence does not occur, if the laser is not resonant with the C-transition. The blue data point corresponds to the laser power chosen for the charge state initialisation measurement in d), while the greyed out data point results from a measurement aborted earlier than the others. **d)** Measurement of the charge state initialisation efficiency. The 445 nm laser pulse of variable pulse length is followed by a 0.5 s long resonant laser pulse with a power chosen such, that electron capture occurs with a probability of 99.9 % for each pulse. The initialisation efficiency is extracted by counting the number of fluorescence response pulses that occur and dividing them by the total number of pulses. For increasing pulse length of the blue laser, the initialisation efficiency follows an exponential law and saturates at 91(1) %.

measurement, the SnV^- centre is permanently charge stabilised by continuous wave 445 nm radiation. The resonance line peak position shift exhibits a standard deviation of less than $4(2)$ MHz and a total width of the summed PLE spectra of $33(2)$ MHz for the whole duration of the measurement, as displayed in Fig.3a). This value has an uncertainty of 2 MHz caused by the uncertainty of our wavemeter which was measured independently. Due to a technical problem of our positioning system within the cryostat, after this measurement, emitter 1 could no longer be accessed. The following measurements were therefore performed on a different emitter (Emitter 2, see supplemental information for characterisation) on which all concepts, that were shown before, work in the same manner. On this SnV^- centre, we investigate the effect of the emitter undergoing the charge cycle by choosing a laser power of 10 nW as a trade-off to ensure continuous electron capture in every single resonance scan while introducing as little as possible power broadening. Even in this case we observe only small shifts in the central resonance position with a standard deviation of $10(2)$ MHz and a total width of the summed PLE spectra of $103(2)$ MHz compared to 88 MHz purely power broadened linewidth, see Fig.3b). The small but visible oscillations with a period of about 10 min in the central resonance position are related to the air conditioning cycle in our laboratory. We consequently claim that the shift is caused by tiny alterations of the position of the blue laser on the sample with respect to the emitter, since slightly misaligning the blue laser spot on the sample has similar effects. This is in agreement with a spatially asymmetric charge distribution caused by the ionised divacancies. This effect has the potential of a tuning mechanism of <100 MHz in resonance frequency, limited by imperfect charge initialisation for strongly misaligned blue laser light. It is remarkable that contrary to the observations reported in [16], the charge stabilisation enables us to limit spectral fluctuations to less than 16% (11%) of the homogeneous (power broadened) linewidth over the course of one hour. For the shifts observed in the low power measurement, even for photons separated by any time distance within the one hour measurement, a Hong-Ou-Mandel Visibility close to 90% would be achievable [29]. Thus, the photons emitted by a charge stabilised SnV^- centre should be highly indistinguishable, which is a key factor in many QIP protocols and quantum communication.

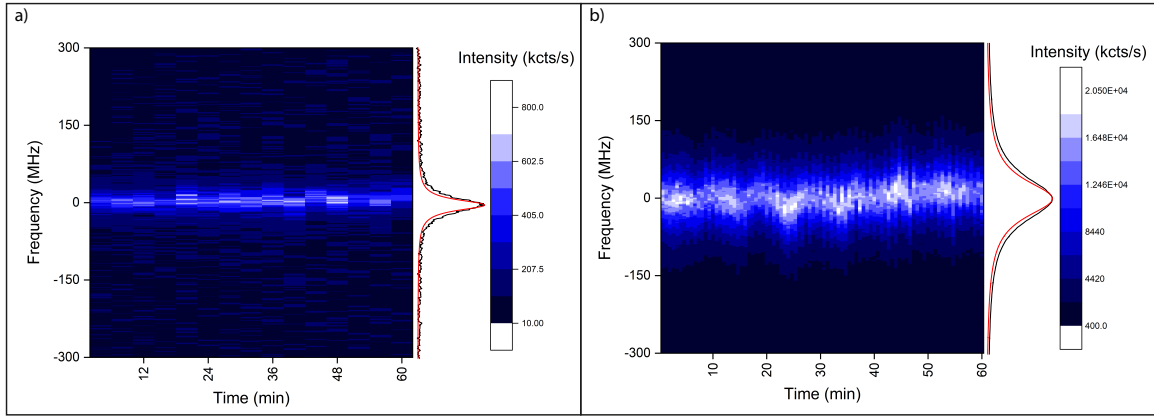


Figure 3: **Longterm stability of the C-transition of SnV^- centres:** a) Low excitation power of 0.5 nW longterm PLE in order to resolve spectral shifts caused by the charge environment or the 445 nm laser without initiating the charge cycle of the centre. The constantly charge stabilised emitter's line position exhibits a standard deviation of less than $4(2)$ MHz over one hour of measurement. On the right, the integrated spectrum over all scans (black) with a width of $33(2)$ MHz is compared with the Fourier limited Lorentzian line (red, 25 MHz) b) Longterm PLE on Emitter 2 with a power of 10 nW ensuring electron capture in every resonance scan while minimising power broadening. In the duration of one hour, the central resonance position exhibits a standard deviation of $10(2)$ MHz. The oscillations with a period of about 10 min in the central resonance position are related to the air conditioning cycle in our laboratory. On the right, the integrated spectrum over all scans (black) with a width of $103(2)$ MHz is compared to a Lorentzian that is only subject to power broadening (red) and exhibits a width of $88(2)$ MHz.

Coherent population trapping

With the means of a stable SnV^- centre resonance line at hand, we explore the possibility of all-optical coherent manipulation of its spin degree of freedom. To this end, we perform CPT between the states $|1 \downarrow\rangle$, $|2 \uparrow\rangle$ via the excited state $|A \downarrow\rangle$. In order to lift the degeneracy of the spin states, we apply a magnetic field $B=0.2$ T at an angle of 54.7° relative to the axis of the defect. When applying a magnetic field to the SnV^- centre, the splitting of the spin states and the long ground state spin T_1 time, which we measure to be larger than 20 ms at 200 mT and 1.7 K (see supplemental material) lead to a vanishing PLE signal due to optical pumping. Introduction of a weak population repump laser at 532 nm leads to the recovery of the PLE signal of the spin conserving (SC) transitions, while the spin flipping (SF) transitions are so weak, that they can be found only via CPT measurements. This is following directly from the isolated atom like selection rules that are a result of the low strain environment and the strong spin-orbit coupling in comparison with the Jahn-Teller effect present for the SnV^- centre [3]. To generate the light fields for CPT we set the carrier laser frequency resonant to the SF transition A2 and we generate the second laser field with the first harmonic of an electro optical phase modulator (EOM). An exemplary characteristic single scan CPT signal is shown in Fig.4a), which is fitted using a three level density matrix formalism (see supplemental material). We relate count rate to populations of the excited state in the following way: In PLE scans with an excitation power $P \gg P_{\text{sat}}$ and without a magnetic field being applied, we measure a fluorescence rate of ~ 45 kcts/s into the phonon sideband, which corresponds to the limit of incoherent pumping and therefore relates to 50% of the population residing in the excited state. This gives us an estimate for the relation of measured count rate to population. A more exact value under the given experimental setting is derived by conducting a high power CPT measurement, shown in Fig.4a) and fitting it with our model. The mismatch of the simulation and the data on the high frequency side of the measurement is caused by approaching the edge of the amplification range of the microwave amplifier used, therefore effectively changing the power in the sideband during the scan. We subsequently decrease the laser power stepwise and change the ratio between control and signal field via the applied microwave power to the EOM. These sets of measurements are used to step by step eliminate free parameters in the fit such as the ratios between Rabi frequencies and laser power, the branching ratio between SC and SF transitions and the exact number of dark counts resulting from background fluorescence of the sample induced by the blue laser light and the dark counts of the avalanche photo diodes (APD) which can be found in the supplemental material. Finally the most interesting parameter, the spin ground state decoherence rate is fitted and yields a value of $64(10)$ kHz, see Fig.4b). This relates to a spin coherence time of $T_2^* = 5(1) \mu\text{s}$ which is slightly larger than found in [1, 3]. In comparison to [1], the branching ratio η between SC and SF transitions amounts to $\sim 650(100)$, which is about a factor 8 larger. This is due to working with an emitter in a nearly unstrained diamond environment.

We wish to emphasize that coherent optical spin control via CPT on an unstrained emitter in a clean diamond environment is only possible using the charge stabilisation method introduced in the previous section. We furthermore would like to point out that this principle worked straightforwardly on several emitters.

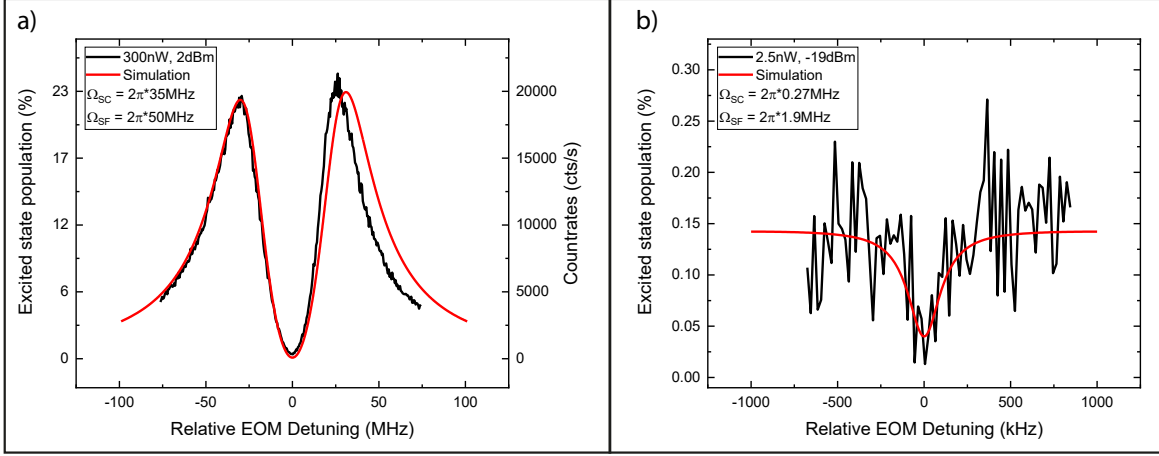


Figure 4: **CPT measurement on a charge stabilised SnV⁻ centre:** **a)** CPT measurement on Emitter 2 with 300 nW of total laser power. This measurement is used to relate measured count rate to excited spin state populations of the SnV⁻ centre. The mismatch of the simulation and the data on the high frequency side of the measurement is caused by approaching the edge of the amplification range of the microwave amplifier used, thereby effectively decreasing the sideband laser power. **b)** Measurement of the CPT dip width with lowest possible total laser power, while preserving a reasonable signal to noise ratio. The data is fitted with a ground state decoherence rate of 64(10) kHz relating to a spin dephasing time of $T_2^* = 5(1) \mu\text{s}$.

Single shot readout

As an outlook to further applications, we investigate whether the strong selection rules, that are described in the previous section, lead to sufficiently strong cycling transitions even when the magnetic field is applied at a large angle with respect to the symmetry axis of the SnV⁻ centre. To this end, we probe the cyclicity by investigating the possibility of a single shot readout. The experiment consists of an 200 μs long initialisation pulse resonant with the SC transition A1 and a 200 μs read pulse on the SC transition B2. As it can be seen in Fig.5a), we achieve an initialisation efficiency of 98.9(4) % in state $|2 \uparrow\rangle$ while detecting an average of 1.21 (1.13) photons per pulse without (with) dark count subtraction. This number is derived from comparing the photons collected in the 200 μs read out interval to the 11139 readout pulses send on to the emitter. We furthermore extract a histogram of photon counts in the readout time interval and compare it to a time interval of the same length where no laser pulse was applied (see Fig.5b)). We extract the readout fidelity following the definition in [30] and set a threshold of one detected photon for a state readout to be detected as bright, while no detected photon corresponds to the state to be dark. The readout error for a bright state to be detected as dark is $\epsilon_B = 0.45$, while the readout error for a dark state to be detected as bright can be extracted from the dark pulse measurement with additionally taking into account the 1.1 % of residual population resulting from imperfect state initialisation, which yields $\epsilon_D = 0.08$. From the averaged state readout error $\epsilon = \frac{1}{2}(\epsilon_B + \epsilon_D)$ we calculate the total readout fidelity as $\mathcal{F} = 1 - \epsilon = 0.74$. This readout fidelity of 74 % surpasses the threshold of 50 % above which a meaningful readout can be implemented, thus demonstrating the potential of the SnV⁻ centre's strong cycling transitions. The readout fidelity can be further improved by using superconducting nanowire single photon detectors which have an improved dark count rate of below 1 Hz compared to 100-200 Hz of the APDs used in our experiments. Furthermore, since our total collection efficiency from bulk diamond is below 1% there are straightforward measures to improve the number of collected photons and thereby enabling high fidelity single shot readout without the necessity of an aligned magnetic field.

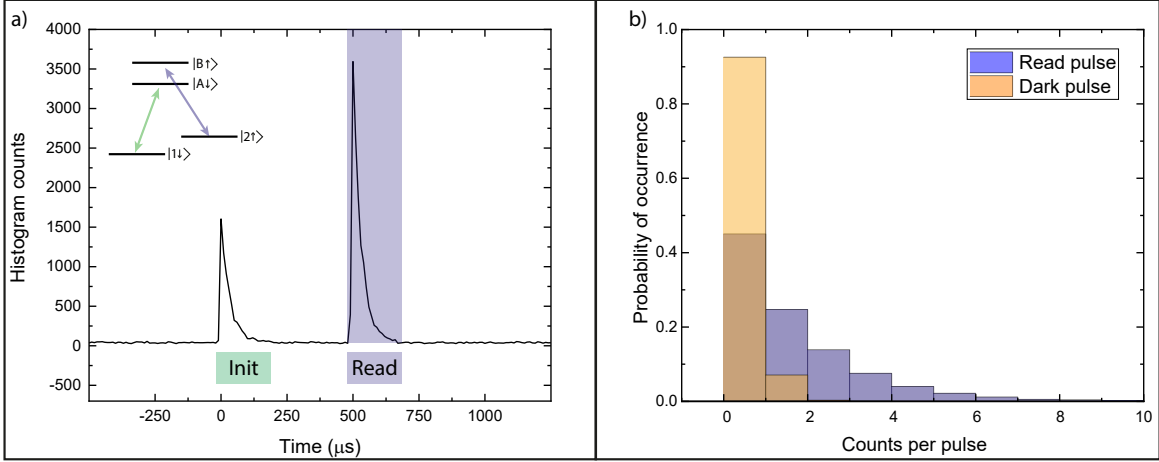


Figure 5: **Single shot readout measurement on a charge stabilised SnV⁻ centre:** **a)** Histogram of the single shot readout measurement on Emitter 2. The 200 μs long initialisation pulse resonant with the A1 transition initialises the spin with an efficiency of 98.9(4) % in the state $|2 \uparrow\rangle$. For each 200 μs long read pulse we detect an average of 1.21 (1.13) photons without (with) dark count subtraction. **b)** Histogram of photon counts in the readout time interval compared to a time interval of the same length where no laser pulse was applied. The overlap of the two measurements, while taking the imperfect state initialisation into account, yields a total readout fidelity of 74 % when setting 1 photon count as a threshold for a state to be detected as bright.

Discussion

In this work, we thoroughly investigated the charge processes taking place for SnV⁻ centres in diamond. We find a dominant single photon electron capture process of single SnV⁻ centres while being in the excited state as the reason for termination of fluorescence under resonant excitation. We propose a charge cycle model universal to G4V centres, which explains the charging and de-charging in the presence of an additional divacancy defect. Based on this model we demonstrate a highly efficient charge initialisation exceeding 90 % utilising a laser with a wavelength of 445 nm as a charge repump. The charge stabilised single SnV⁻ centres are investigated in terms of the long term stability of the resonance line with and without undergoing a full charge cycle. We find that the charge stabilisation preserves very stable optical transitions with deviations of the line centers well below the lifetime-limited linewidth over the duration of one hour in both cases. Furthermore, we probe the spin coherence of a charge stabilised SnV⁻ centre and find a spin lifetime $T_1 > 20$ ms and a spin dephasing time of $T_2^* = 5(1) \mu\text{s}$ at a temperature of 1.7 K. As an outlook for further applications, we implement a single shot readout scheme which yields a readout fidelity of 74 %, demonstrating the highly cycling spin conserving transitions even in the case of a large angle of 54.7° between magnetic field and the symmetry axis of the defect. It is straightforward to increase the readout fidelity by implementing means to improve the total collection efficiency of our optical setup such as utilising optical antennas [31], micropillars [3], solid immersion lenses, or photonic crystal structures [32, 33]. In summary, we have shown that the charge stabilisation protocol developed in this work renders the SnV⁻ centre suitable for reliable application in QIP, in which well defined charge states, longterm stable optical resonances for the emission of highly indistinguishable photons, long spin coherence times and efficient state readout are absolutely crucial.

Methods

Sample preparation

The predominantly investigated sample NI58 is an (001) electronic grade bulk diamond which is homogeneously implanted with tin ions at an implantation energy of 700 keV and a fluence of $8 \times 10^{13} \frac{\text{Ions}}{\text{cm}^2}$. A subsequent annealing at 2100°C and 7.7 GPa is employed to reduce implantation damage. A detailed

characterisation of the sample can be found in [2]. The second sample BOJO_001, which is investigated in the supplemental material, is produced by tin ion implantation at an implantation energy of 700 keV and 4 different fluences ranging from $10^9 \frac{\text{Ions}}{\text{cm}^2}$ to $10^{12} \frac{\text{Ions}}{\text{cm}^2}$. A subsequent annealing 2100°C and 8 GPa for 2 h strongly reduces implantation damage.

Experimental setup

The measurements were conducted in a home built confocal microscope with the sample being situated inside an closed cycle helium cryostat (attodry2100, attocube systems AG) which operates at a base temperature of ~ 1.7 K. The sample is moved via a combination of stepper (2x ANPx51, ANPz51, attocube systems AG) and scanner positioners (ANSxy50, attocube systems AG). We use an NA 0.9 objective (MPLN100x, Olympus) for photon collection.

The second wavelength for the fluorescence enhancement measurement is retrieved from a super-continuum laser source (SuperK FIANIUM FIU-15, NKT Photonics) with ~ 100 ps long pulses and with a bandwidth of 10 nm. The resonant laser fields are generated from a side of fringe stabilised Dye cw laser (Matisse 2DS, Sirah Lasertechnik GmbH) which can be locked to a wavemeter (WS6-200, HighFinesse GmbH), while the laser light at 445 nm is emitted by a diode laser (Cobolt 06-MLD, Hübner Photonics). Pulses are carved from the cw lasers using acousto optical amplitude modulators (AOM, AOMO 3200-146, Crystal Technology).

The timing of the pulse sequences for the ionisation, charge initialisation and single shot readout experiments is controlled via an digital delay generator (DG645, Stanford Research Systems).

The optical sidebands for the CPT experiments are introduced by an electro-optical phase modulator (EOM, WPM-K0620, AdvR). The microwave signals used to drive this modulator are emitted from an microwave generator (mg3692c, Anritsu) and sent through a microwave amplifier (ZHL-42+, Mini-Circuits).

For the single shot readout, a second microwave generator (SG384, Stanford Research Systems) is employed in order to implement two sidebands with frequencies resonant with both SC transitions. The sidebands are switched using two microwave switches (ZASW-2-50DRA+, Mini-Circuits).

Data availability

The underlying data for this manuscript is openly available in Zenodo at <http://doi.org/10.5281/zenodo.5561219>. The evaluation algorithms are available from the corresponding author upon reasonable request.

References

- [1] Debroux, R. *et al.* Quantum control of the tin-vacancy spin qubit in diamond. *arxiv* (2021). 2106.00723.
- [2] Görlitz, J. *et al.* Spectroscopic investigations of negatively charged tin-vacancy centres in diamond. *New Journal of Physics* **22**, 013048 (2020). URL <https://doi.org/10.1088/1367-2630/ab6631>.
- [3] Trusheim, M. E. *et al.* Transform-limited photons from a coherent tin-vacancy spin in diamond. *Phys. Rev. Lett.* **124**, 023602 (2020). URL <https://link.aps.org/doi/10.1103/PhysRevLett.124.023602>.
- [4] Pompili, M. *et al.* Realization of a multinode quantum network of remote solid-state qubits. *Science* **372**, 259–264 (2021). URL <https://science.sciencemag.org/content/372/6539/259>. <https://science.sciencemag.org/content/372/6539/259.full.pdf>.
- [5] Nguyen, C. T. *et al.* Quantum network nodes based on diamond qubits with an efficient nanophotonic interface. *Phys. Rev. Lett.* **123**, 183602 (2019). URL <https://link.aps.org/doi/10.1103/PhysRevLett.123.183602>.
- [6] Bhaskar, M. K. *et al.* Experimental demonstration of memory-enhanced quantum communication. *Nature* **580**, 60–64 (2020). URL <https://doi.org/10.1038/s41586-020-2103-5>.

- [7] Sukachev, D. D. *et al.* Silicon-vacancy spin qubit in diamond: A quantum memory exceeding 10 ms with single-shot state readout. *Phys. Rev. Lett.* **119**, 223602 (2017). URL <https://link.aps.org/doi/10.1103/PhysRevLett.119.223602>.
- [8] Neu, E. *et al.* Single photon emission from silicon-vacancy colour centres in chemical vapour deposition nano-diamonds on iridium. *New Journal of Physics* **13**, 025012 (2011). URL <https://doi.org/10.1088/1367-2630/13/2/025012>.
- [9] Rogers, L. J. *et al.* Multiple intrinsically identical single-photon emitters in the solid state. *Nature Communications* **5**, 4739 (2014). URL <https://doi.org/10.1038/ncomms5739>.
- [10] Bhaskar, M. K. *et al.* Quantum nonlinear optics with a germanium-vacancy color center in a nanoscale diamond waveguide. *Phys. Rev. Lett.* **118**, 223603 (2017). URL <https://link.aps.org/doi/10.1103/PhysRevLett.118.223603>.
- [11] van Dam, S. B. *et al.* Optical coherence of diamond nitrogen-vacancy centers formed by ion implantation and annealing. *Phys. Rev. B* **99**, 161203 (2019). URL <https://link.aps.org/doi/10.1103/PhysRevB.99.161203>.
- [12] Fu, K.-M. C., Santori, C., Barclay, P. E. & Beausoleil, R. G. Conversion of neutral nitrogen-vacancy centers to negatively charged nitrogen-vacancy centers through selective oxidation. *Applied Physics Letters* **96**, 121907 (2010). URL <https://doi.org/10.1063/1.3364135>.
- [13] De Santis, L., Trusheim, M. E., Chen, K. C. & Englund, D. R. Investigation of the stark effect on a centrosymmetric quantum emitter in diamond. *Phys. Rev. Lett.* **127**, 147402 (2021). URL <https://link.aps.org/doi/10.1103/PhysRevLett.127.147402>.
- [14] Aghaeimeibodi, S., Riedel, D., Rugar, A. E., Dory, C. & Vučković, J. Electrical tuning of tin-vacancy centers in diamond. *Phys. Rev. Applied* **15**, 064010 (2021). URL <https://link.aps.org/doi/10.1103/PhysRevApplied.15.064010>.
- [15] Nguyen, C. T. *et al.* An integrated nanophotonic quantum register based on silicon-vacancy spins in diamond. *Phys. Rev. B* **100**, 165428 (2019). URL <https://link.aps.org/doi/10.1103/PhysRevB.100.165428>.
- [16] Rugar, A. E. *et al.* Narrow-linewidth tin-vacancy centers in a diamond waveguide. *ACS Photonics* **7**, 2356–2361 (2020). URL <https://doi.org/10.1021/acsp Photonics.0c00833>. <https://doi.org/10.1021/acsp Photonics.0c00833>.
- [17] Iwasaki, T. *et al.* Tin-vacancy quantum emitters in diamond. *Phys. Rev. Lett.* **119**, 253601 (2017). URL <https://link.aps.org/doi/10.1103/PhysRevLett.119.253601>.
- [18] Tchernij, S. D. *et al.* Single-photon-emitting optical centers in diamond fabricated upon Sn implantation. *ACS Photonics* **4**, 2580–2586 (2017). URL <https://doi.org/10.1021/acsp Photonics.7b00904>.
- [19] Thiering, G. & Gali, A. Ab initio magneto-optical spectrum of group-IV vacancy color centers in diamond. *Phys. Rev. X* **8**, 021063 (2018). URL <https://link.aps.org/doi/10.1103/PhysRevX.8.021063>.
- [20] Chen, D. *et al.* Optical gating of resonance fluorescence from a single germanium vacancy color center in diamond. *Phys. Rev. Lett.* **123**, 033602 (2019). URL <https://link.aps.org/doi/10.1103/PhysRevLett.123.033602>.
- [21] Becker, J. N. *et al.* All-optical control of the silicon-vacancy spin in diamond at millikelvin temperatures. *Phys. Rev. Lett.* **120**, 053603 (2018). URL <https://link.aps.org/doi/10.1103/PhysRevLett.120.053603>.
- [22] Siyushev, P. *et al.* Optical and microwave control of germanium-vacancy center spins in diamond. *Phys. Rev. B* **96**, 081201 (2017). URL <https://link.aps.org/doi/10.1103/PhysRevB.96.081201>.

- [23] Thiering, G. & Gali, A. The $(eg \otimes eu) \otimes eg$ product jahn–teller effect in the neutral group-iv vacancy quantum bits in diamond. *npj Computational Materials* **5**, 18 (2019). URL <https://doi.org/10.1038/s41524-019-0158-3>.
- [24] Gardill, A. *et al.* Probing charge dynamics in diamond with an individual color center. *Nano Letters* **21**, 6960–6966 (2021). URL <https://doi.org/10.1021/acs.nanolett.1c02250>. PMID: 34339601, <https://doi.org/10.1021/acs.nanolett.1c02250>.
- [25] Deák, P., Aradi, B., Kaviani, M., Frauenheim, T. & Gali, A. Formation of NV centers in diamond: A theoretical study based on calculated transitions and migration of nitrogen and vacancy related defects. *Phys. Rev. B* **89**, 075203 (2014). URL <https://link.aps.org/doi/10.1103/PhysRevB.89.075203>.
- [26] Pu, A., Avalos, V. & Dannefaer, S. Negative charging of mono-and divacancies in Ila diamonds by monochromatic illumination. *Diamond and Related Materials* **10**, 585–587 (2001). URL <https://www.sciencedirect.com/science/article/pii/S0925963500004416>. 11th European Conference on Diamond, Diamond-like Materials, Carbon Nanotubes, Nitrides and Silicon Carbide.
- [27] Dobrinets, I. A., Vins, V. G. & Zaitsev, A. M. *HPHT-treated diamonds*, vol. 181 (Springer-Verlag Berlin Heidelberg, 2013). URL <https://www.springer.com/gp/book/9783642374890>.
- [28] Slepetz, B. & Kertesz, M. Divacancies in diamond: a stepwise formation mechanism. *Phys. Chem. Chem. Phys.* **16**, 1515–1521 (2014). URL <http://dx.doi.org/10.1039/C3CP53384K>.
- [29] Kambs, B. & Becher, C. Limitations on the indistinguishability of photons from remote solid state sources. *New Journal of Physics* **20**, 115003 (2018). URL <https://doi.org/10.1088/1367-2630/aaea99>.
- [30] Myerson, A. H. *et al.* High-fidelity readout of trapped-ion qubits. *Phys. Rev. Lett.* **100**, 200502 (2008). URL <https://link.aps.org/doi/10.1103/PhysRevLett.100.200502>.
- [31] Fuchs, P., Jung, T., Kieschnick, M., Meijer, J. & Becher, C. A cavity-based optical antenna for color centers in diamond. *APL Photonics* **6**, 086102 (2021). URL <https://doi.org/10.1063/5.0057161>. <https://doi.org/10.1063/5.0057161>.
- [32] Kuruma, K. *et al.* Coupling of a single tin-vacancy center to a photonic crystal cavity in diamond. *Applied Physics Letters* **118**, 230601 (2021). URL <https://doi.org/10.1063/5.0051675>.
- [33] Rugar, A. E. *et al.* Quantum photonic interface for tin-vacancy centers in diamond. *Phys. Rev. X* **11**, 031021 (2021). URL <https://link.aps.org/doi/10.1103/PhysRevX.11.031021>.

Acknowledgements

We thank Elke Neu and Richard Nelz for providing the additional microwave source and for fruitful discussions. We thank Adam Gali and Jero Maze for helpful theoretical insight and discussions on the charge cycle of colour centres in diamond.

This research received funding from the European Union’s Horizon 2020 research and innovation programme under Grant Agreement No. 820394 (ASTERIQS), the EMPIR programme co-financed by the Participating States and from the European Union’s Horizon 2020 research and innovation programme (Project No. 17FUN06 SIQUST), the German Federal Ministry of Education and Research (Bundesministerium für Bildung und Forschung, BMBF) within the projects Q.Link.X (Contract No. 16KIS0864) and QR.X (Contract No. 16KISQ001K) and the Deutsche Forschungsgemeinschaft (DFG, German Research FoundaHon) -- Project-ID 429529648 -- TRR 306 QuCoLiMa (“Quantum Cooperativity of Light and Matter”).

T.I. and M.H. acknowledge the Toray Science Foundation and the MEXT Quantum Leap Flagship Program (MEXT Q-LEAP) (Grant No. JPMXS0118067395).

T.T. acknowledges support from MEXT Q-LEAP (Grant No. JPMXS0118068379) and JSPS KAKENHI (Grant No. JP20K21096).

Author contributions

J.G. and D.He. designed and J.G. conceived the experiment. J.G., D.He., P.F. and C.B. discussed and designed the charge cycle model. T.I. and T.T. prepared the main sample, D.R., J.G., D.He., D.Ha. and P.-O. C. prepared the additional HPHT sample. M.H. and M.M. supervised the HPHT sample preparation for the two samples. C.B. supervised the whole project. The paper was written with input from all authors.

Competing interests

The authors declare no competing interests.

Materials and correspondence

C.B. and J.G. should be addressed for correspondence and material requests. Email: christoph.becher@physik.uni-saarland.de; j.goerlitz@physik.uni-saarland.de

Supplementary information

Supplementary information is available for this paper at XXX.